Model-Based Analysis of the ZrO_2 Etching Mechanism in Inductively Coupled BCl_3/Ar and BCl_3/CHF_3/Ar Plasmas

Mansu Kim, Nam-Ki Min, Sun Jin Yun, Hyun Woo Lee,
Alexander M. Efremov, and Kwang-Ho Kwon

The etching mechanism of ZrO_2 thin films and etch selectivity over some materials in both BCl_3/Ar and BCl_3/CHF_3/Ar plasmas are investigated using a combination of experimental and modeling methods. To obtain the data on plasma composition and fluxes of active species, global (0-dimensional) plasma models are developed with Langmuir probe diagnostics data. In BCl_3/Ar plasma, changes in gas mixing ratio result in non-linear changes of both densities and fluxes for Cl, BCl_2, and BCl_2^+. In this work, it is shown that the non-monotonic behavior of the ZrO_2 etch rate as a function of the BCl_3/Ar mixing ratio could be related to the ion-assisted etch mechanism and the ion-flux-limited etch regime. The addition of up to 33% CHF_3 to the BCl_3-rich BCl_3/Ar plasma does not influence the ZrO_2 etch rate, but it non-monotonically changes the etch rates of both Si and SiO_2. The last effect can probably be associated with the corresponding behavior of the F atom density.

Keywords: ZrO_2, etch rate, dissociation, ionization, etch mechanism, BCl_3/Ar and BCl_3/CHF_3/Ar plasma modeling.

Manuscript received July 16, 2007; revised Jan. 12, 2008.

Mansu Kim (email: happytv@korea.ac.kr), Nam-Ki Min (email: nkmin@korea.ac.kr), and Kwang-Ho Kwon (phone: + 82 41 860 1447, email: kwonkh@korea.ac.kr) are with the Department of Control and Instrumentation Engineering, Korea University, Chungnam, Rep. of Korea.

Sun Jin Yun (email: sjyun@etri.re.kr) is with the Convergence Components & Materials Research Laboratory, ETRI, Daejeon, Rep. of Korea.

Hyun Woo Lee (email: hwlee@hanseo.a.c.kr) is with the Department of Computer and Applied Physics, Hanseo University, Seosan, Rep. of Korea.

Alexander M. Efremov (email: efremov@isuct.ru) is with the Department of Electronic Devices & Materials Technology, Ivanovo State University of Chemistry & Technology, Ivanovo, Russia.

I. Introduction

Plasma etching of high dielectric constant (high-*k*) materials is an issue of increasing concern due to integration of these materials in sub-0.1 μm complementary metal oxide semiconductor (CMOS) technology [1]. Among the known high-*k* materials, ZrO_2 attracts great attention because of its high dielectric constant (k is 20 to 25), wide bandgap (around 5 to 7 eV) as well as a close thermal expansion coefficient with Si that results in good thermal stability of the ZrO_2/Si structures. Therefore, the development of an anisotropic etch process for ZrO_2 thin films is important.

There have only been a few works devoted to the investigation of the etching behavior of ZrO_2 thin films using chlorine-based plasma chemistries. In particular, Sha and Chang reported on an etch process for ZrO_2 thin film in both Cl_2 and Cl_2/BCl_3 plasmas [2], while Pelhos and others investigated the etch behavior of $Zr_{1-x}Al_xO_y$ thin film in Cl_2/BCl_3 plasma [3]. Although these works show the dependence of the ZrO_2 etch rate on gas pressure, input power, and bias power, the relationships between process parameters, plasma chemistry, and surface kinetics were not explored well. In fact, only Sha and Chang [2] attempted the model-based analysis of the ZrO_2 etch mechanism in the BCl_3/Cl_2 plasma and obtained a relatively good agreement between measured and model-predicted etch rates. However, their model suffers from an excess of free fitting parameters and has a pure agreement with the basic theory of ion-assisted chemical etching [4]. That is why the ZrO_2 etch mechanism is not clearly

understood and this retards further integration of this material in CMOS technology. Another critical issue to be investigated and optimized is the etch selectivity of ZrO_2 over the commonly used substrate and mask materials. It is known that a highly-selective etch process allows a smaller feature size and an accurate pattern transfer to be obtained.

In this work, we investigate the etch mechanism of ZrO_2 thin films as well as the etch selectivity over Si and SiO_2 in an inductively coupled plasma (ICP) system with BCl_3/Ar and BCl_3/CHF_3/Ar gas chemistries. The BCl_3 was chosen as an active gas because it is widely used for the etching of the materials covered by the native oxides due to the effective extraction of oxygen in the form of BCl_xO_y compounds [5]. The addition of CHF_3 to the BCl_3/Ar plasma was aimed at investigating the influence of the F-containing gas on the etch selectivities over Si and SiO_2. To analyze the ZrO_2 etch mechanism, the models of plasma chemistry and surface kinetics were developed.

II. Experiment

1. Experimental Setup and Procedures

The 130-nm thick ZrO_2 films were deposited on Si (100) substrates at 150°C by a plasma-enhanced atomic layer deposition (PEALD) method. Detailed descriptions of both the deposition method and operating conditions are given in [6]. Si (100) and SiO_2 substrates were used to determine ZrO_2/Si and ZrO_2/SiO_2 selectivity.

Etching experiments were performed in a planar ICP reactor (see Fig. 1). The reactor consisted of a cylindrical quartz chamber with a radius (r) of 16 cm and a 5-turn copper coil located on a 10-mm-thick horizontal quartz window. The coil was connected to a 13.56 MHz power supply. The distance between the quartz window and the bottom electrode (l) used as a substrate holder was 12.8 cm. The bottom electrode was also connected to a 13.56 MHz power supply to control dc bias voltage on the substrate. During the etch process, the temperature of the substrate holder was held at 17°C by the circulation of deionized water. The etching conditions were the following: a gas pressure (p) of 5 mTorr, an input ICP power (W) of 500 W, and bias power (W_{dc}) of 100 W. The initial compositions of the BCl_3/Ar gas mixtures were set by adjusting the partial flow rate of the components within the total flow rate (q) of 60 sccm. For the three-component BCl_3/CHF_3/Ar system, the CHF_3 was added to the 25/5 sccm BCl_3/Ar gas mixture, so that a total gas flow rate was varied in the range from 30 sccm to 45 sccm.

The etched ZrO_2 samples had an area of 2×2 cm^2. To determine the etch rate and etch selectivity, the etched depths of

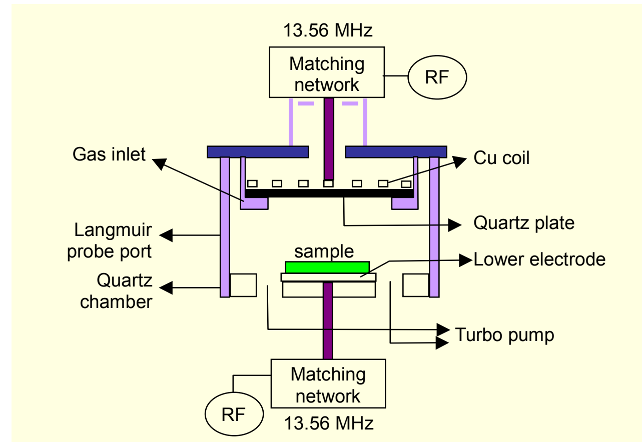

Fig. 1. Schematic drawing of the ICP etching reactor.

ZrO_2 and Si were measured using a surface profiler (Alpha-step 500, KLA-Tencor Corp.).

Plasma diagnostics were performed by double Langmuir probe (DLP2000, Plasmart Inc.) measurements. The probes were installed through the view-port on the side wall of the reactor chamber and centered in a radial direction. For the treatment of voltage-current curves aimed to obtain electron temperature and ion density, we used the software supplied by the equipment manufacturer.

2. 0-Dimensional Plasma Models

To obtain data on the densities and fluxes of plasma active species, we used a simplified global (0-dimensional) model with a Maxwellian electron energy distribution function (EEDF) and with a quasi-stationary approximation for the volume kinetics [7], [8]. The applicability of the Maxwellian approximation for EEDFs in BCl_3, Ar, and CHF_3 inductive discharges at low pressures was demonstrated in [9] and [10] by an outstanding agreement between plasma diagnostics data and modeling results. The modeling algorithm was based on the simultaneous solution of the following equations.

- The balance equations for neutral and charged species in a steady-state dn/dt=0 approximation R_F–R_D=$\nu_G n$, where R_F and R_D are the average rates of formation and decay in plasma volume, n is the volume-average density of particles, and ν_G is the frequency (first-order rate coefficients) of the heterogeneous decay. The list of processes taken into account by the model was composed using [9], [11], and [12] and is shown in Tables 1 to 3.
- The quasi-neutrality conditions for the volume densities of charged particles (n_e+n_-=n_+, where $n_+ \approx n_{BCl_2^+} + n_{Ar^+}$) and for their fluxes to the reactor wall (Γ_e=Γ_+).

As the input parameters for modeling, we used the experimental data on electron temperature (T_e) and total

Table 1. Reaction set for the BCl_3 plasma modeling.

Process		ε_{th} (eV)	Rate coefficient
Dissociation and dissociative attachment			
R1	$BCl_3 + e \rightarrow BCl_2 + Cl + e$	4.61	$1.27\times10^{-4}T_e^{-0.908}\exp(-70886/T_e)$
R2	$BCl_3 + e \rightarrow BCl + 2Cl + e$	5.65	$2.14\times10^{-4}T_e^{-0.937}\exp(-79765/T_e)$
R3	$BCl_3 + e \rightarrow BCl_2 + Cl^+ + 2e$	23.45	$3.81\times10^{-10}T_e^{0.434}\exp(-266700/T_e)$
R4	$BCl_3 + e \rightarrow BCl_2 + Cl^-$	0.14	$2.18\times10^{-4}T_e^{-1.301}\exp(-10749/T_e)$
R5	$BCl_2 + e \rightarrow BCl + Cl + e$	4.61	$1.27\times10^{-4}T_e^{-0.908}\exp(-70886/T_e)$
R6	$BCl + e \rightarrow B + Cl + e$	4.61	$1.27\times10^{-4}T_e^{-0.908}\exp(-70886/T_e)$
R7	$Cl_2 + e \rightarrow Cl + Cl + e$	3.0	$2.11\times10^{-9}T_e^{0.232}\exp(-54886/T_e)$
R8	$Cl_2 + e \rightarrow Cl + Cl^-$	-	$2.33\times10^{-11}T_e^{0.237}\exp(-9163.8/T_e)$
R9	$Cl_2 + BCl_2 \Leftrightarrow BCl_3 + Cl$		$1.00\times10^{-11}\exp(-600/T)$
R10	$Cl_2 + BCl \Leftrightarrow BCl_2 + Cl$		$9.60\times10^{-11}\exp(-610/T)$
R11	$Cl_2 + B \Leftrightarrow BCl + Cl$		$7.90\times10^{-10}\exp(-780/T)$
Ionization and dissociative ionization			
R12	$BCl_3 + e \rightarrow BCl_2^+ + Cl + 2e$	12.6	$7.54\times10^{-9}T_e^{0.290}\exp(-150110/T_e)$
R13	$BCl_3 + e \rightarrow BCl^+ + 2Cl + 2e$	20.02	$2.39\times10^{-8}T_e^{-0.054}\exp(-237490/T_e)$
R14	$BCl_2 + e \rightarrow BCl_2^+ + 2e$	10.1	$1.03\times10^{-9}T_e^{-0.213}\exp(-122160/T_e)$
R15	$BCl + e \rightarrow BCl^+ + 2e$	10.3	$5.4\times10^{-10}T_e^{-0.211}\exp(-124230/T_e)$
R16	$Cl_2 + e \rightarrow Cl_2^+ + 2e$	11.5	$1.02\times10^{-10}T_e^{0.641}\exp(-150810/T_e)$
R17	$Cl + e \rightarrow Cl^+ + 2e$	13.5	$5.09\times10^{-10}T_e^{0.457}\exp(-155900/T_e)$
Recombination of ions			
R18	$Cl^- + N_+ \rightarrow N + Cl$	-	1.0×10^{-7}
R19	BCl_2^+, BCl^+, Cl_2^+, $Cl^+ \rightarrow$ wall	-	υ_B/d_c
Recombination of neutrals			
R20	N + wall $\rightarrow$ N(s), where N = BCl_2 / BCl / Cl / B	-	0.1 / 0.2 / 0.5 / 1 (sticking coeff.)
R21	N + N(s) $\rightarrow$ N-N		from [10]
R22	$B + BCl_2(s) \rightarrow BCl(s) + BCl$		0.05
R23	$BCl + BCl_2(s) \rightarrow BCl(s) + BCl_2$		0.02

positive ion density (n_+) extracted from the Langmuir probe measurements.

For all neutral non-saturated dissociation products (F, CF_x, O), we accounted for the Eley-Rideal heterogeneous recombination kinetics with $\nu_G = \left[\left(\Lambda^2/D\right) + \left(2r/0.25\gamma\upsilon_T\right)\right]^{-1}$ [10], where $\Lambda = \left[\left(2.405/r\right)^2 + \left(\pi/l\right)^2\right]^{-1/2}$ is the diffusion length, γ is the sticking or recombination probability, and $\upsilon_T = \left(8k_BT/\pi m\right)^{1/2}$. The effective diffusion coefficients, D, were calculated as $D^{-1} = D_f^{-1} + D_{in}^{-1}$, where $D_f = (\Lambda/3)(8k_BT/\pi m)^{1/2}$ is the free diffusion coefficient, and D_{in} is the inter-diffusion coefficient given by the Chapman-Enskog equation together with Blanc's law [7]. For negative ions, we assumed ν_G=0 due to the presence of a double electric layer and of the negative charges on the reactor walls made from dielectric materials [7], [8]. For positive ions, we used $\nu_G \approx \upsilon/d_c$ where $d_c = 0.5rl/(rh_l + lh_r)$. The ion Bohm velocities υ were calculated from $\upsilon = \sqrt{eT_e(1+\beta_s)/m_i(1+\beta_s\gamma_T)}$ [8], where $\gamma_T = T_e/T_i$, and β_s is the relative density of

Table 2. Simplified reaction set for the CHF_3 plasma modeling.

Process		ε_{th} (eV)	Rate coefficient
Dissociation and dissociative attachment			
R24	$CHF_3 + e \rightarrow F + CHF_2 + e$	13.0	$1.403\times10^{-8} T_e^{0.359} \exp(-11.373/T_e)$
R25	$CHF_3 + e \rightarrow H + CF_3 + e$	11.0	$9.309\times10^{-9} T_e^{0.2041} \exp(-11.423/T_e)$
R26	$CHF_2 + e \rightarrow CHF + F + e$	4.75	$1.403\times10^{-8} T_e^{0.359} \exp(-11.373/T_e)$
R27	$CHF_2 + e \rightarrow H + CF_2 + e$	2.71	$9.309\times10^{-9} T_e^{0.2041} \exp(-11.423/T_e)$
R28	$CHF + e \rightarrow H + CF + e$	3.30	$9.309\times10^{-9} T_e^{0.2041} \exp(-11.423/T_e)$
R29	$CF_3 + e \rightarrow CF_2 + F + e$	3.8	$4.163\times10^{-4} T_e^{-0.9407} \exp(-1.301\times10^{5}/T_e)$
R30	$CF_2 + e \rightarrow CF + F + e$	5.4	$1.19\times10^{-16} T_e^{1.31} \exp(-1.446\times10^{5}/T_e)$
R31	$CF + e \rightarrow C + F + e$	5.6	$1.19\times10^{-16} T_e^{1.31} \exp(-1.446\times10^{5}/T_e)$
R32	$HF + e \rightarrow H + F + e$	5.85	$3.625\times10^{-8} T_e^{-0.313} \exp(-13.139/T_e)$
R33	$CHF_3 + e \rightarrow CHF_2 + F^-$		$1.11\times10^{-7} T_e^{-1.2306} \exp(-42190/T_e)$
R34	$CF_3 + e \rightarrow CF_2 + F^-$	0.4	$2.369\times10^{-8} T_e^{-0.4893} \exp(-58760/T_e)$
R35	$HF + e \rightarrow H + F^-$		$1.87\times10^{-12} T_e^{0.237} \exp(-9159.9/T_e)$
R36	$CHF_3 + F \rightarrow HF + CF_3$		1.49×10^{-13}
R37	$CHF_2 + F \rightarrow HF + CF_2$		4.98×10^{-11}
R38	$CHF_2 + H \rightarrow HF + CHF$		4.43×10^{-10}
R39	$CF_3 + H \rightarrow HF + CF_2$		9.11×10^{-11}
R40	$CF_2 + H \rightarrow HF + CF$		3.90×10^{-11}
R41	$CF + H \rightarrow HF + C$		1.90×10^{-11}
Recombination of ions			
R42	$F^- + N_+ \rightarrow N + F$	-	1.0×10^{-7}
Recombination of neutrals			
R43	N + wall $\rightarrow$ N(s), where N = CHF_2 / CHF / CF_3 / CF_2 / CF/ F / H	-	(sticking coeff.) 0.2 / 0.2 / 0.1 / 0.5 / 0.5 / 0.3 / 0.3
R44	N + N(s) $\rightarrow$ N-N		from [12], see also text

For R24-R28, R30, R31, R33-R35, T_e is in eV. For all other electron impact reactions, T_e is in K.

Table 3. Additional reaction set for BCl_3/Ar and BCl_3/CHF_3/Ar plasma modeling.

Process		ε_{th} (eV)	Rate coefficient
R45	$Ar + e \rightarrow Ar^+ + 2e$	15.8	$7.07\times10^{-11} T_e^{0.232} \exp(-64886/T_e)$
R46	$HCl + e \rightarrow H + Cl + e$	4.5	$1.45\times10^{-10} T_e^{0.245} \exp(-53886/T_e)$
R47	$HCl + e \rightarrow H + Cl^-$	0.4	$2.33\times10^{-11} T_e^{0.237} \exp(-10111/T_e)$
R48	$HCl + F \rightarrow HF + Cl$		8.7×10^{-11}
R49	$CHF_3 + Cl \rightarrow HCl + CF_3$		3.3×10^{-14}
R50	$CHF_2 + Cl \rightarrow HCl + CF_2$		3.3×10^{-14}
R51	$CHF + Cl \rightarrow HCl + CF$		3.3×10^{-14}
R52	H + Cl(s) $\rightarrow$ HCl		see text
R53	Cl + H(s) $\rightarrow$ HCl		see text

negative ions at the plasma sheath edge. The last parameters are connected with bulk electronegativity $\beta = n_-/n_e$ as $\beta_s = \beta\left[\exp\left((1+\beta_s)(\gamma_T - 1)/2(1+\beta_s\gamma_T)\right)\right]^{-1}$. For simplicity, we assumed the temperature of all kinds of ions to be equal and dependent only on the gas pressure; thus, $T_i \approx T + (0.5 - T)/p$, where T is the gas temperature in V and p is the pressure in mTorr [7]. The coefficients h_l and h_r are given by the low pressure $\lambda \le (T_i/T_e)(R, L)$ diffusion theory [7], [13] as $h_l \approx 0.86\left(1 + 2\beta_s\gamma_T^{-1}/1+\beta_s\right)\left(3 + (l/2\lambda)\right)^{-1/2}$ and $h_r \approx 0.80(1 + 3\beta_s\gamma_T^{-1}/1+\beta_s)\left(4 + (r/\lambda)\right)^{-1/2}$, where $\lambda^{-1} = \sum y_i\lambda_i^{-1}$ is the averaged ion mean free path, while y_i and λ_i are a mole fraction (inside n_+) and a partial free path for each kind of positive ion. The partial values of λ_i were estimated as $\lambda_i = \sum(\sigma_{i-n}N_i)^{-1}$, where σ_{i-n} denotes the ion-neutral interaction cross-sections and N_i denotes the partial densities of neutral species. The parameters σ_{i-n} were determined using the polarizability data for neutral species [14] and assuming the charge transfer process is the main mechanism for ion scattering in bulk plasma.

3. Phenomenological Model of Etch Kinetics

To analyze the ZrO_2 etch mechanism, we used a simplified model of etch kinetics based on the theory of active surface sites [15], [16]. The assumptions were formulated as follows: 1) Cl or F atoms are the main chemically active species; 2) the formation of low volatile Zr chlorides or fluorides is the main channel for the loss of active surface sites; 3) the contribution of physical sputtering of ZrO_2 by Ar^+ ions can be neglected; and 4) all kinds of positive ions are effective for the ion-stimulated desorption of reaction products. In such a situation, the total etch rate can be expressed as $R = \delta s_0\Gamma_N(1-\theta)$, where δ is the stoichiometry coefficient (for example, δ = 0.25 for $ZrCl_4$); s_0, which is around 0.3 to 0.5, [15], [16] is the sticking coefficient for etchant species; $\Gamma_N = 0.25 n_N(8k_BT/\pi m_N)^{1/2}$ is the flux of neutral species with the volume density of n_N; and θ is the fraction of surface sites covered by the reaction products. The stationary balance for the free surface sites $(1-\theta)$ is given by $\delta s_0\Gamma_N(1-\theta) = \theta\sum Y_{d,i}\Gamma_{+,i}$. Thus, we can write

$$R = \delta s_0\Gamma_N\left(1 - \frac{\delta s_0\Gamma_N}{\delta s_0\Gamma_N + \sum Y_{d,i}\Gamma_{+,i}}\right), \qquad (1)$$

where $\Gamma_{+,i} \approx h_l n_{+,i}\left(eT_e/m_i\right)^{1/2}$ are the partial fluxes for positive ions with densities of n_{+i}, and $Y_{d,i} = A\left(\sqrt{\varepsilon} - \sqrt{\varepsilon_0}\right)$ [16] are the partial desorption yields. Parameter A is the constant depending on the type of incident ion, ε_0 is the desorption threshold, and ε is the incident ion energy, which is the sum of ion acceleration energy in the plasma sheath (about $5.2T_e$ for pure Ar plasma and about $6.3T_e$ for pure BCl_3 plasma, assuming BCl_2^+ is the dominant ion) and the negative dc bias voltage applied to the substrate. The parameters A, which is around 0.04 to 0.06, and ε_0, around 21 eV, for BCl_2^+ ions can be derived from [2]. For other ions (Cl^+, Ar^+, and so on), we assumed the same desorption thresholds but recalculated the A values proportionally to the momentum transferred to the surface in a single collision.

III. Results and Discussion

1. BCl_3/Ar Plasma

For the given composition of the bulk plasma, the etch kinetics depends strongly on such factors as reaction probability and sputtering/desorption yields for both native atoms and reaction products. The experimental data on the saturated vapor pressures for $ZrCl_x$ are absent, but we can refer to the corresponding melting points (T_m) assuming a qualitative correlation of these parameters with the volatility [14]. From [2] and [14], we can find that T_m = 772°C and 437°C for $ZrCl_2$ and $ZrCl_4$, respectively. Therefore, we can neglect the spontaneous desorption of reaction products and assume that the ion-assisted chemical reaction is the main etch mechanism in the BCl_3-rich plasma. Also, since the Zr-O bond is stronger than the Zr-Cl bond (8.06 eV versus 5.11 eV [2]), the direct chlorination of the ZrO_2 surface at near-to-room temperature seems to be impossible. That is why the role of ion bombardment includes, at least, the destruction of the Zr-O bonds to support the formation of $ZrCl_x$ and the sputtering of the $ZrCl_x$ layer to provide the access of Cl atoms to the etched surface. Although it was reported in [2] that the Cl atoms were the main etchant for ZrO_2 in Cl-containing both BCl_3 and Cl_2 plasmas, some additional effect can result from the unsaturated BCl_x radicals. The strength of the B-O bond is 8.4 eV [2], so the spontaneous reactions $2BCl_x + ZrO_2 \rightarrow Zr + 2BOCl_x$ are easily expected. In fact, such a process liberates the metal from the oxide and accelerates the formation of Zr chlorides. At the same time, the etch kinetics and threshold (determined from the dependence of the etch rate on $\sqrt{\varepsilon}$) for ZrO_2 in Cl_2 and BCl_3 plasmas are very close [2]. This means that the BCl_x works as a catalyst but not as the main chemically active species.

From Fig. 2, it can be seen that an increase in the Ar mixing ratio results in the non-linear behavior of the ZrO_2 etch rate. In particular, for 16% to 83% Ar, the etch rate changes weakly in the range from 36.9 to 31.4 nm/min, whereas in pure Ar

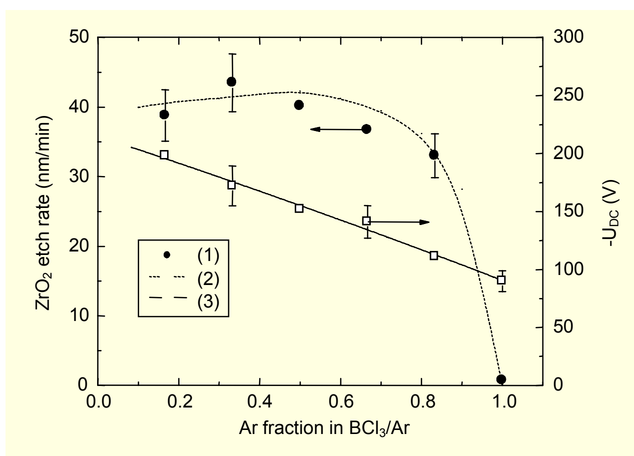

Fig. 2. (1) Experimental and (2) model predicted ZrO_2 etch rates as well as (3) negative dc bias as functions of BCl_3/Ar mixing ratio (*p*=5 mTorr, *q*=60 sccm). Solid line is to guide the eye only.

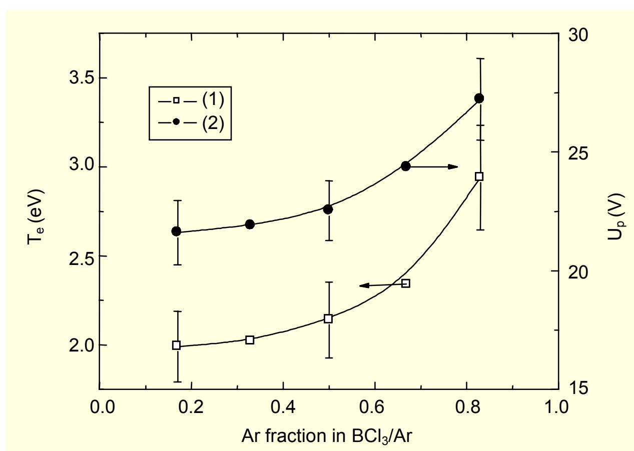

Fig. 3. (1) Experimental data on electron temperature and (2) plasma potential as functions of BCl_3/Ar mixing ratio (*p*=5 mTorr, *q*=60 sccm). Solid lines are to guide the eye only.

plasma, it drops down to 0.65 nm/min. This probably results from the low ZrO_2 sputtering yield and the decreasing dc bias on the etched sample (224 to 158 V for 10% to 90% Ar). In fact, this makes it possible to neglect the contribution of sputtering by Ar^+ even in the Ar-rich plasma. The ZrO_2/Si etch selectivity keeps a near-to-constant value of 1.15 to 0.92 for 17% to 83% Ar. This means that there is a quite close etch kinetics (and thus, etch mechanisms) for both ZrO_2 and Si that is in good agreement with our assumptions on the ZrO_2 etch mechanism.

Figures 3 and 4 illustrate the influence of the BCl_3/Ar mixing ratio on both plasma parameters and densities of active species. An increase in the Ar mixing ratio from 17% to 83% results in an increasing electron temperature in the range from 1.99 eV to 2.94 eV (see Fig. 3) that is in good agreement with published data [17].

A similar effect has been repeatedly mentioned in the literature for Cl_2/Ar plasma [18]-[20]. It is caused by the domination of the high-threshold process in the reaction set for Ar atoms. The rate coefficients of R1 to R7 and R12 to R17 follow the behavior of T_e, while the main source of Cl atoms is represented by the dissociation BCl_3 through R1 and R2. The contributions of R12 and R13 are much lower due to high threshold of the dissociative ionization process. Accordingly, the effective dissociation rate coefficient (k_1+2k_2) occupies the range of (1.9 to 5.9)×10^{-9} cm^3/s for 17% to 83% Ar, and the Cl atom formation frequency (k_1+2k_2)n_e changes in the range from 161 to 954 s^{-1}. As a result, both the BCl_3 dissociation rate and the Cl atom density (see Fig. 4(a)) fall more slowly than those to be expected from the change of the initial mixture composition. The density of BCl_2 radicals is lower than the density of Cl atoms because of the lower formation rate: $(k_1+2k_2)/(k_1+k_3+k_4)$ is around 2.2 to 2.7 and n_{Cl}/n_{BCl_2} is around 2.0 to 2.6 for 17% to 83% Ar. Also, the density of BCl radicals is much lower than the Cl and BCl_2 densities. The main source of BCl is represented by R2, while the decay rate is higher than those for Cl and BCl_2 due to a higher sticking coefficient and a higher surface polymerization ability [9]. As a result, we obtain a n_{BCl_2}/n_{BCl} value of around 3.9 to 2.0 for 17% to 83% Ar. All of these are in good agreement with the published data on diagnostics and modeling of the BCl_3-containing plasmas [9], [17], [21], [22].

As shown in Fig. 4(b), an increase in the Ar mixing ratio causes the same effects for both n_+ (1.29×10^{11} to 1.82×10^{11} cm^{-3} for 17% to 83% Ar) and n_e (8.27×10^{10} to 1.72×10^{11} cm^{-3} for 17% to 83% Ar). This can be attributed to the increasing total ionization rate (1.810^{15} to 8.910^{15} $cm^{-3}s^{-1}$ for 17% to 83% Ar) and the change of the total balance of charged particles determined by the quasi-neutrality condition. The density of Cl^- follows the behavior of the R4 rate and decreases monotonically in the range from 4.6×10^{10} to 9.6×10^{9} cm^{-3} that provides a value of 0.6 to 0.05 for n_{Cl^-}/n_e . The last value is in good agreement with the published data for low-pressure electronegative plasmas, including the BCl_3 ICP [18]-[20]. Among the positive ions, the dominant one is the BCl_2^+ with $n_{BCl_2^+}/n_{Ar^+}$ around 302 to 14 and $n_{BCl_2^+}/n_{Cl^+}$ around 52 to 14 for 17% to 83% Ar, while the density of BCl_2^+ exceeds that of BCl^+ by an order of magnitude. All of these result from the differences in partial ionization rates (in particular, BCl_2^+ is formed directly from the BCl_3 molecules) and the faster decay of other ions due to lower mass and higher ion Bohm velocity. It is also important to note that the density of BCl_2^+ changes non-monotonically with an increasing Ar mixing ratio. This is caused by the corresponding behavior of the formation rate for

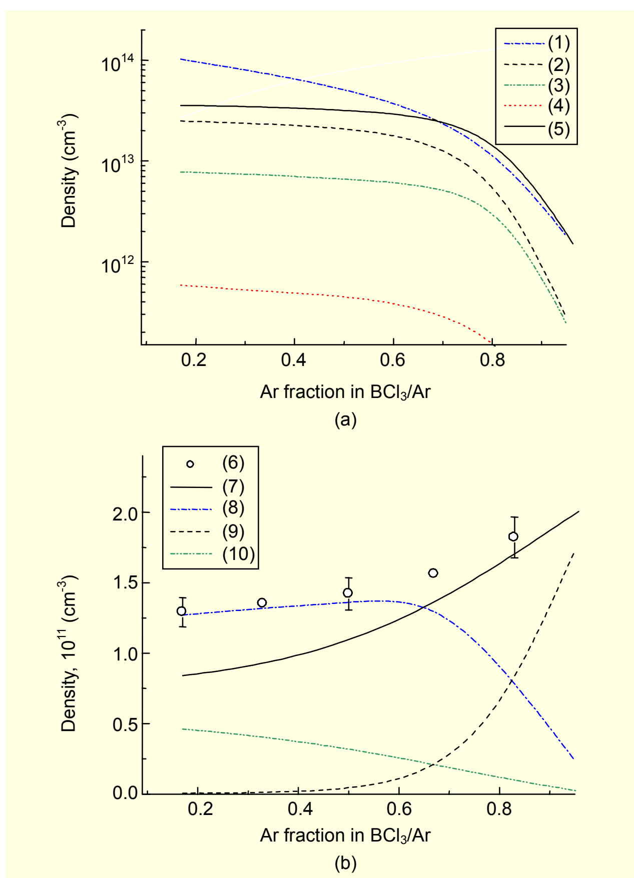

Fig. 4. Model-predicted densities of (a) neutral and (b) charged species in the BCl_3/Ar plasma: (1) – BCl_3, (2) – BCl_2, (3) – BCl, (4) – Cl_2, (5) – Cl, (6) – total density of positive ions determined by LP measurements, (7) – electrons, (8) – BCl_2^+, (9) – Ar^+, and (10) – Cl^-.

BCl_2^+ (R12+R14) due to the concurrence between the decreasing volume densities of neutral species and increasing n_e and ionization rate coefficients.

The comparison of the experimental data on the ZrO_2 etch rate (see Fig. 2) and the model-predicted plasma composition (see Fig. 4) shows an evident correlation between relative behavior of the etch rate and the BCl_2^+ density. Generally, this seems reasonable since the ZrO_2 etch mechanism represented by ion-assisted chemical reaction and the rate of the whole process are limited by the ion-stimulated desorption of reaction products. To analyze this situation in detail, we applied the simplified model of etch kinetics described in Section II.3. It was found that the main role in ion-stimulated desorption of reaction products belongs to BCl_2^+ with $(Y_d\Gamma)_{BCl_2^+}/(Y_d\Gamma)_{Ar^+}$ around 300 to 1.4 for 17% to 83% Ar. An increase in the Ar mixing ratio lowers the fraction of chlorinated surface (θ is 0.77 to 0.61 for A=0.1 and θ is 0.97 to 0.91 for A=0.01 at 17% to 83% Ar), but the fraction of free surface (1–θ) does not exceed 40% for A=0.1 and 8% for A=0.01 even at 80% Ar. This is due to a high chlorination rate ($\sum Y_{d,i}\Gamma_{+,i}/\delta s_0\Gamma_{Cl}$ equals to 0.16 to 0.27 with A = 0.05 at 17% to 83% Ar) supported by a non-linearly slow decrease in Γ_{Cl} with an increasing Ar mixing ratio. Taking into account that for $\delta s_0\Gamma_{Cl} >> \sum Y_{d,i}\Gamma_{+,i}$ (1) gives $R \to \sum Y_{d,i}\Gamma_{+,i}$, it is understandable why the ZrO_2 etch rate follows the behavior of the BCl_2^+ density and flux. In fact, we have the ion-flux-limited etch regime, where the total etch rate is limited by the ion-stimulated desorption of low volatile reaction products. Also, using δs_0, which is 0.02 to 0.03, A = 0.042 (that is in good agreement [2]), and multiplying the result of (1) by a factor of $6\times10^8 M/\rho N_a$ (M = 123.2 g/mol is the ZrO_2 molar mass, ρ = 5.68 g/cm^3 is the ZrO_2 atom density, and N_a = 6.02×10^{23}), we obtain 40 nm/min, 42 nm/min, and 32 nm/min at 17%, 50%, and 83% Ar, respectively. Since the model-predicted curve seen as a dashed line in Fig. 2 agrees with an experimental one in both relative and absolute scales, we can assume that the sets of assumptions for plasma chemistry and etch kinetics used to build the models provide an adequate description of the ZrO_2 etch mechanism.

As explained in [23] and [24], the etch mechanisms of both Si and SiO_2 in chlorine-containing plasma also follow the ion-assisted chemical reaction. That is why the ZrO_2/Si and ZrO_2/SiO_2 etch selectivities in the BCl_3/Ar plasma cannot be principally improved by variations of input process parameters. One way to adjust the etch selectivity is to complement the BCl_3/Ar gas mixture with another active gas providing the formation of more volatile products for one of the etched substances. For this purpose, we investigated the effect of adding CHF_3 to the 25/5 sccm BCl_3/Ar gas mixture.

2. BCl_3/CHF_3/Ar Plasma

Figure 5 shows that, as the CHF_3 mixing ratio in the BCl_3/Ar plasma increases up to 33%, the ZrO_2 etch rate shows a weak tendency to decrease in the range from 38.8 to 38.1 nm/min. Since the difference between maximum and minimum values lies within the margin of experimental error, a conclusion about the constant ZrO_2 etch rate seems reasonable. From [14], it can be seen that the volatility of Zr fluorides is much lower than that of corresponding chlorides (T_m = 932°C for ZrF_4), while the strength of the Zr-F bond (6.4 eV) is lower than that of the Zr-O bond. The negative dc bias on the substrate also keeps a near-to-constant value, so that the obtained behavior of the ZrO_2 etch rate is in agreement with the ion-assisted etch mechanism previously proposed. In other words, the addition of CHF_3 to the BCl_3/Ar plasma provides no evident reasons to accelerate the chemical etch pathway or to change the ion-flux-limited etch regime. At the same time, the etch rates of both Si

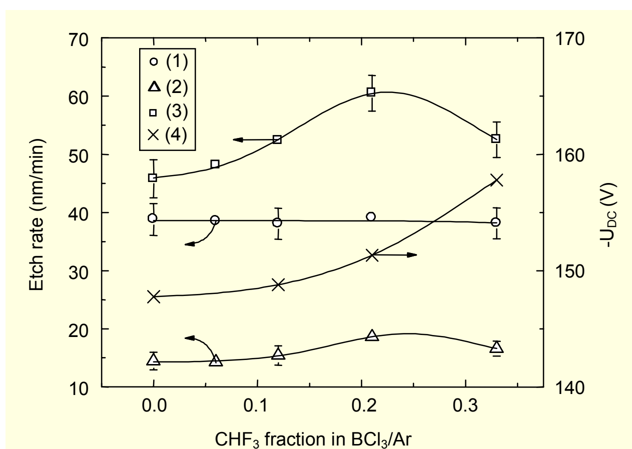

Fig. 5. (1) Etch rates of ZrO_2, (2) SiO_2, and (3) Si as well as (4) negative dc bias on the substrate as functions of CHF_3 mixing ratio in BCl_3/Ar plasma (p=5 mTorr, q=30-45 sccm). Solid line is to guide the eye only.

and SiO_2 exhibit a higher sensitivity to the addition of CHF_3 in the BCl_3/Ar plasma and increase from 45.8 to 60.5 nm/min and from 14.5 to 18.8 nm/min, respectively, for 0% to 20% CHF_3. However, the further addition of CHF_3 results in the Si and SiO_2 etch rates decreasing to 52.5 nm/min and 16.5 nm/min at 33% CHF_3. Generally, this also looks reasonable since the spontaneous reaction of F atoms with these materials occurs even at near-to-room temperatures [5], [13].

Before analyzing the parameters and composition for the BCl_3/CHF_3/Ar plasma, we would like to mention some peculiarities of this system. First, the cross sections for electron impact processes involving CHF_3 and corresponding dissociation fragments are not known with appropriate accuracy [12]. In fact, there are only two works devoted to the modeling of the CHF_3 plasma [11], [12]. They used different sets of process and different sets of cross sections, and they obtained different results on plasma composition. The second problem is that the heterogeneous chemistry is not well understood yet. This particularly relates to unknowns for both sticking coefficients for CHF_x(x<3) and the dominant recombination pathway with adsorbed species. Finally, there is no detailed experimental data on CHF_3 plasma composition; therefore, no plasma models have adequacy criteria. (the quality of a model cannot be evaluated by comparison with experiment). When developing the model for the CHF_3 plasma, we used the following assumptions. First, compared with the reaction sets from [11] and [12], we reduced the kinetic scheme of electron impact reaction and left only the processes really influencing the particle balance for the given range of experimental conditions (Table 2) Second, the sticking coefficients for CHF_2 and CHF were taken from [11] and [25] like those for CF_2 and CF. Third, for the given adsorbed particle,

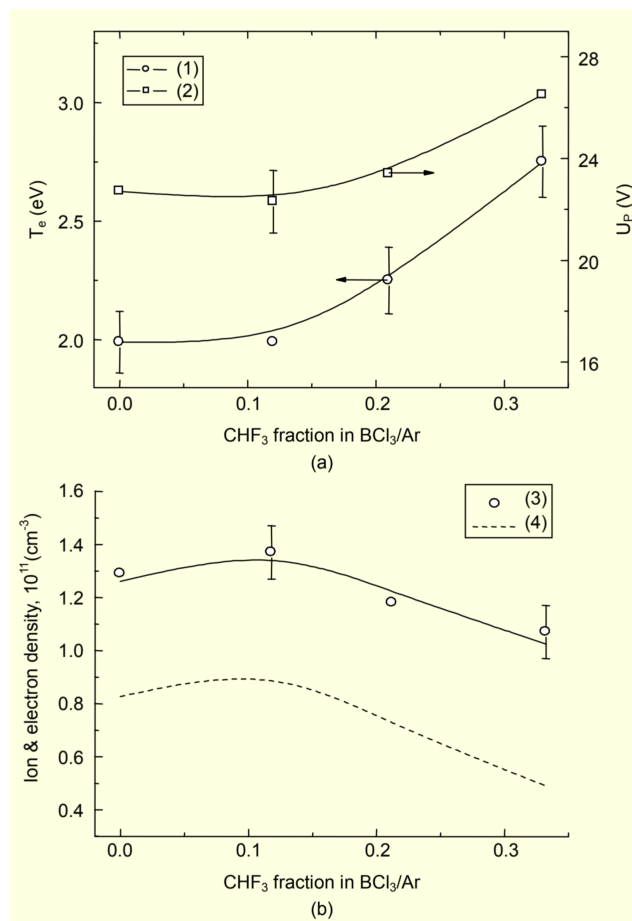

Fig. 6. (a) Plasma parameters and (b) densities of charged species as functions of CHF_3 mixing ratio in BCl_3/Ar plasma (p=5 mTorr, q=30-45 sccm): (1) – electron temperature, (2) – plasma potential, (3) – total positive ion density, and (4) – electron density. Solid lines are to guide the eye only.

all recombination pathways with other unsaturated components were equalized by assuming equal partial probabilities. Finally, the balance equations for positive ions were not solved. In fact, we solved only the balance equations for negative ions and derived n_e from known n_+ using the quasi-neutrality condition. Taking into account the simplifications previously mentioned, the modeling results for the BCl_3/CHF_3/Ar plasma should be viewed on a relative scale rather than on an absolute one.

Figure 6 illustrates the influence of the CHF_3 mixing ratio on the plasma parameters and densities of charged species. As the CHF_3 mixing ratio in the BCl_3/Ar plasma increases from 0% to 33%, the electron temperature also increases in the range between 1.99 to 2.75 eV. This phenomenon seems reasonable because the CHF_3 and many sub-products have higher excitation and ionization potentials than those of BCl_3 and Ar.

The total density of positive ions (see Fig. 6(b)) exhibits a weak maximum at 10% CHF_3; however, it then decreases by a

factor of 1.2 compared with pure BCl_3/Ar plasma. Although the rate coefficient for CHF_3 is lower than that for BCl_3 (1.14×10^{-12} to 1.27×10^{-12} cm^3/s for 0% to 33% CHF_3), the formation of negative ions is noticeably influenced by such highly-electronegative species as CF_3, HF, and HCl. That is why an increase in the CHF_3 mixing ratio increases the total density of negative ions and increases the gap between n_+ and n_e (n_-/n_e is 0.56 to 1.18, where $n_- = n_{Cl^-} + n_{F^-}$, and n_+/n_e is 1.56 to 2.18). With this background, the non-monotonic behaviors of both n_+ and n_e are not surprising and can be associated with their increasing decay rates through the dissociative attachments R34, R35, and R47 (see Tables 2 and 3) and ion-ion recombinations R18 and R42. The modeling results also show that a specific feature of the CHF_3 plasma is the high density of CF_3 and HF (see Fig. 7(a)), and this fact is in good agreement with [11] and [12]. As shown in Table 2, these species appear in fast atom-molecular reactions R36 to R41 resulting in the effective consumption of both F and H atoms. As a result, the densities of mentioned atomic species are noticeably lower than those of CF_3 and HF. Also, the mixing of CHF_3 with a chlorine-containing environment opens several pathways for the formation of HCl (R49 to R51 in Table 3) and, simultaneously, increases the decay of F atoms by increasing the rate of R48. That is why the density of F atoms changes non-monotonically (see Fig. 7(b)) and exhibits a quite clear maximum at 21% to 23% CHF_3 in the BCl_3/Ar plasma. In our opinion, this fact can be accepted as a qualitative proof for the non-monotonic behaviors of the Si and SiO_2 etch rates.

The analysis of the ZrO_2 etch kinetics in the BCl_3/CHF_3/Ar plasma is generally a problem because of the multi-component composition of bulk plasma, which includes such possible etchants as Cl, F, CF_x, HF, and HCl. However, taking into account that the Cl atoms dominate over other mentioned species (see Fig. 7(b)), we neglected any chemical effects except ones from the Cl. Accordingly, we assumed $\Gamma_N = \Gamma_{Cl}$ in (1). As for the behavior of the Cl atom density, this parameter decreases monotonically in the range of (3.44 to 2.15)$\times10^{13}$ cm^{-3} for 0% to 33% CHF_3 (see Fig. 7(b)). As the modeling results demonstrate, the slow decrease of n_{cl} is caused by the action of two factors: the increasing dissociation rate coefficient due to increasing electron temperature and the effective re-generation of Cl atoms through the reactions involving HCl. For the case of $\delta s_0 \Gamma_{Cl} >> \sum Y_{d,i} \Gamma_{+,i}$ (that is, $(1-\theta) << 1$), the etch rate has low sensitivity to changes in the flux of chemically active species. For this reason, it seems reasonable that the change of Cl atom density has no similar influence on the ZrO_2 etch rate. The analysis of ionization kinetics using the reaction set from [12] makes it possible to conclude that, for the given set of experimental conditions, the dominant positive

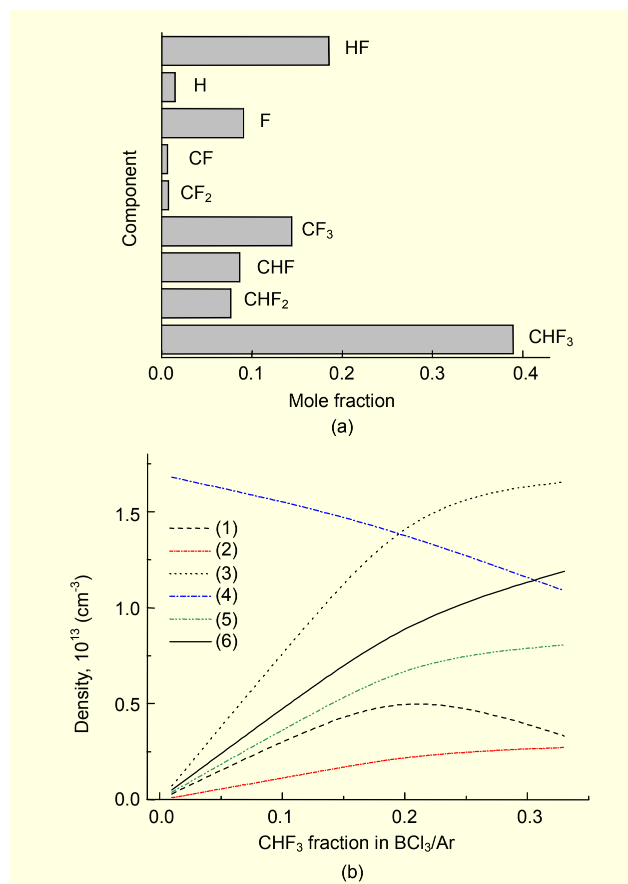

Fig. 7. (a) Model-predicted composition of pure CHF_3 plasma (p=5 mTorr, T_e=2 eV, and $n_e=8\times10^{10}$ cm^{-3}) and (b) densities of neutral species in the BCl_3/CHF_3/Ar plasma: (1) – F, (2) –CF_2, (3) – CF_3, (4) – Cl (lowered by a factor of 2 to fit the scale), (5) – HCl, and (6) – HF.

ions are BCl_2^+ and CF_3^+ with quite close masses. Evaluation of the net flux of positive ions $\Gamma_+ \approx h_l n_+ \left(eT_e/m_i\right)^{1/2}$ reveals that as the CHF_3 mixing ratio increases the second and third multiplicands work in opposite directions; therefore, the change in Γ_+ is expected to be insufficient. This allow us to assume a near-to-constant efficiency of ion-stimulated desorption of reaction products and explains the constancy of the ZrO_2 etch rate demonstrated by the experiments. Therefore, the model of the ion-assisted etch mechanism described in section II.3 gives a qualitative explanation of the ZrO_2 etch behavior with the addition of CHF_3 to the BCl_3/Ar plasma. More accurate analysis will be possible involving the experimental data on the CHF_3 plasma composition to adjust the uncertain reaction pathways.

Finally, we would like to note one more time that our models of plasma chemistry and etch kinetics, especially for the BCl_3/CHF_3/Ar plasma, cannot provide an accurate quantitative analysis of the ZrO_2 etching mechanism for all cases due to some simplifications and uncertainties in primary assumptions.

However, the model-based analysis enhances the understanding of the relationships between input process parameters and the etch rate, illustrates the relative contributions of both chemical and physical etch pathways, and determines the factors of primary influence on the process characteristics.

IV. Conclusion

In this work, we investigated the etch mechanism of ZrO_2 thin films and etch selectivity over Si and SiO_2 in BCl_3/Ar and BCl_3/CHF_3/Ar inductively coupled plasmas. For this purpose, we used a combination of experimental and modeling methods. To obtain the data on plasma composition and fluxes of active species, global (0-dimensional) plasma models were developed with the Langmuir probe diagnostics data as input parameters. It was shown that an increase of the Ar mixing ratio in the BCl_3/Ar plasma resulted in non-linear changes of both densities and fluxes for Cl and BCl_2^+. From the model-based analysis of surface kinetics, it was shown that the non-monotonic behavior of the ZrO_2 etch rate as a function of the BCl_3/Ar mixing ratio could be explained within the assumption of the ion-assisted etch mechanism and the ion-flux-limited etch regime. The addition of CHF_3 to the BCl_3-rich BCl_3/Ar plasma up to 33% does not influence the ZrO_2 etch rate, but it non-monotonically changes the etch rates of both Si and SiO_2. This last effect can probably be associated with the corresponding behavior of the F atom density. For this reason, we obtained a degradation of both ZrO_2/Si and ZrO_2/SiO_2 etch selectivities in the F-containing plasmas compared with those for BCl_3/Ar. A method to improve selectivity will be the subject of further research.

References

[1] J.P. Chang, Y.-S. Lin, and K. Chu, "Rapid Thermal Chemical Vapor Deposition of Zirconium Oxide for Metal-Oxide-Semiconductor Field Effect Transistor Application," *J. Vac. Sci. Technol., B*, vol. 19, 2001, pp. 1782-1787.

[2] L. Sha and J.P. Chang, "Plasma Etching of High Dielectric Constant Materials on Silicon in Halogen Chemistries," *J. Vac. Sci. Technol., A*, vol. 22, 2004, pp. 88-95.

[3] K. Pelhos, V. Donnelly, A. Kornblit, M. Green, R. V. Dover, L. Manchanda, Y. Hu, M. Morris, and E. Bower, "Etching of High-*k* Dielectric $Zr_{1-x}Al_xO_y$ Films in Chlorine-Containing Plasmas," *J. Vac. Sci. Technol., A*, vol. 19, 2001, pp. 1361-1366.

[4] L. Stafford and J. Margot, "Comment on "Plasma Etching of High Dielectric Constant Materials on Silicon in Halogen Plasma Chemistries," by L. Sha and J.P. Chang [J. Vac. *Sci. Technol., A*, vol. 22, 88 (2004)]," *J. Vac. Sci. Technol., A*, vol. 23, 2005, pp. 720-721.

[5] J.R. Rooth, *Industrial Plasma Engineering*, IOP Publishing Ltd., Philadelphia, 1995.

[6] S.J. Yun, J.W. Lim, and J.H. Lee, "Effect of Plasma on Characteristics of Zirconium Oxide Films Deposited by Plasma-Enhanced Atomic Layer Deposition," *Electrochem. Solid-State Lett.*, vol. 8, 2005, pp. F47-F50.

[7] C. Lee and M.A. Lieberman, "Global Model of Ar, O_2, Cl_2, and Ar/O_2 High-Density Plasma Discharges," *J. Vac. Sci. Technol., A*, vol. 13, 1995, pp. 368-380.

[8] M.A. Lieberman and S. Ashida, "Global Models of Pulse-Power-Modulated High-Density, Low-Pressure Discharges," *Plasma Sources Sci. Technol.*, vol. 5, 1996, pp. 145-158.

[9] E. Meeks, P. Ho, A. Ting, and R.J. Buss, "Simulations of BCl_3/Cl_2/Ar Plasmas with Comparisons to Diagnostic Data," *J. Vac. Sci. Technol., A*, vol. 16, 1998, pp. 2227-2239.

[10] P.N. Wainman, M.A. Lieberman, A.J. Lichtenberg, R.A. Stewart, and C. Lee, "Characterization at Different Aspect Ratios (radius/length) of a Radio Frequency Inductively Coupled Plasma Source," *J. Vac. Sci. Technol., A*, vol. 13, 1995, pp. 2464-2469.

[11] P. Ho, J.E. Johannes, R.J. Buss, and E. Meeks, "Modeling the Plasma Chemistry of C_2F_6 and CHF_3 Etching of Silicon Dioxide, with Comparisons to Etch Rate and Diagnostic Data," *J. Vac. Sci. Technol., A*, vol. 19, 2001, pp. 2344-2267.

[12] D. Bose, M.V.V.S. Rao, T.R. Govindan, and M Meyyappan, "Uncertainty and Sensitivity Analysis of Gas-Phase Chemistry in a CHF_3 Plasma," *Plasma Sources Sci. Technol.*, vol. 12, 2003, pp. 225-234.

[13] M.A. Lieberman and A.J. Lichtenberg, *Principles of Plasma Discharges and Materials Processing*, John Wiley & Sons Inc., New York, 1994.

[14] D.R. Lide, *Handbook of Chemistry and Physics*, CRC Press, New York, 1998-1999.

[15] C. Lee, D.B. Graves, and M.A. Lieberman, "Role of Etch Products in Polysilicon Etching in a High-Density Chlorine Discharge," *Plasma Chem. and Plasma Proc.*, vol. 16, 1996, pp. 99-120.

[16] A.M. Efremov, D.P. Kim, and C.I. Kim, "Simple Model for Ion-Assisted Etching Using Cl_2–Ar Inductively Coupled Plasma: Effect of Gas Mixing Ratio," *IEEE Trans. Plasma Science*, vol. 32, 2004, pp. 1344-1351.

[17] G.H. Kim, C.-I. Kim, and A.M. Efremov, "Effect of Gas Mixing Ratio on MgO Etch Behaviour in Inductively Coupled BCl_3/Ar Plasma," *Vacuum*, vol. 79, 2005, pp. 231-240.

[18] N.C.M. Fuller, V.M. Donnelly, and I.P. Herman, "Electron Temperatures of Inductively Coupled Cl_2–Ar Plasmas," *J. Vac. Sci. Technol., A*, vol. 20, 2002, pp. 170-173.

[19] A.M. Efremov, D.P. Kim, and C.-I. Kim, "Inductively Coupled Cl_2/Ar Plasma: Experimental Investigation and Modeling," *J. Vac. Sci. Technol., A*, vol. 21, 2003, pp. 1568-1573.

[20] A.M. Efremov, G.H. Kim, J.G. Kim, A.V. Bogomolov, and C.-I. Kim, "On the Applicability of Self-Consistent Global Model for the Characterization of Cl_2/Ar Inductively Coupled Plasma,"

Microelectronic Engineering, vol. 84, 2007, pp. 136-143.

[21] K.J. Nordheden and J.F. Sia, "Characterization of BCl_3/N_2 Plasmas," *J. Appl. Phys.*, vol. 94, 2003, pp. 2199-2202.

[22] H.S. Kim, G.Y. Yeom, J.W. Lee, and T.I. Kim, "Characteristics of Inductively Coupled Cl_2/BCl_3 Plasmas during GaN Etching," *J. Vac. Sci. Technol., A*, vol. 17, 1999, pp. 2214-2219.

[23] S.A. Vitale, H. Chae, and H.H. Sawin, "Silicon Etching Yields in F_2, Cl_2, Br_2, and HBr High Density Plasmas," *J. Vac. Sci. Technol., A*, vol. 19, 2001, pp. 2197-2206.

[24] S. Abdollahi-Alibeik, J.P. McVittie, K.C. Saraswat, V. Sukharev, and P. Schoenborn, "Analytical Modeling of Silicon Etch Process in High Density Plasma," *J. Vac. Sci. Technol., A*, vol. 17, 1999, pp. 2485-2491.

[25] M.V.V.S. Rao, S.P. Sharma, B.A. Cruden, and M. Meyyappan, "Langmuir Probe and Mass Spectrometric Measurements in Inductively Coupled CF_4 Plasmas," *Plasma Sources Sci. Technol.*, vol. 11, 2002, pp. 69-76.

Mansu Kim received his BS degree in the electronic engineering from Hanseo University, Seoul, Korea, in 2006, and his MS degree from Korea University in 2008. His research interests include plasma etching processes, silicon semiconductor processing, and sensor devices.

Nam-Ki Min received the BS and MS degrees in electrical engineering from Korea University, Seoul, Korea, in 1974 and 1976, respectively. He received the PhD degree in electrical engineering from the University of Cincinnati, Cincinnati, OH, in 1989. He is currently a professor with the Electrical Engineering Department, Korea University. He was previously with Dongguk University, Seoul, Korea, in a similar position from 1978 to 1984. His research interests focus on the development of MEMS-based sensors, nanobiosensors, and other sensors for automotive applications.

Sun Jin Yun received her BS degree in chemistry from Pusan National University, Korea, in 1982, and MS, and PhD degrees in chemistry from Korea Advanced Institute of Science and Technology, Seoul, Korea, in 1983 and 1987, respectively. Since 1987, she has worked with ETRI. Also, from 1992 to 1993, she worked as a visiting research associate with the Department of Electrical and Computer Engineering of the University of Illinois at Urbana-Champaign, IL, USA. Her research interests include the fabrication of new functional thin films and the development of sensors and microelectronic devices utilizing engineered thin films.

Hyun Woo Lee received the BS degree from Seoul National University, Seoul, Korea, in 1983, and the PhD degree from Korea Advanced Institute of Science and Technology, Daejeon, Korea in 1991. From 1989 to 1995, was a senior engineer with the Semiconductor R&D Lab of Hyundai Electronics, Inc. Since 1995, he has been an associate professor of Computer and Applied Physics with Hanseo University, Seosan, Korea. He is a member of the Korean Physical Society. His areas of research are plasma diagnostics and plasma modeling of low-temperature plasmas.

Alexander M. Efremov received the ME, PhD and the DSc (full doctor) degrees from Ivanovo State University of Chemistry and Technology, Ivanovo, Russia, in 1989, 1995, and 2005, respectively. From 1995 to 2006, he was with the Department of Electronic Devices and Materials Technology, Ivanovo State University of Chemistry and Technology, where he worked as an associate professor. Also, from 2002 to 2004 and in 2006, he worked as an invited researcher and visiting professor for the Plasma Application Laboratory of the School of Electrical and Electronic Engineering, Chung-Ang University, Seoul, Korea. Since 2006, he has been with Ivanovo State University of Chemistry and Technology, where he is currently a full professor of the Department of Electronic Devices and Materials Technology. His research interests include plasma modeling and the analysis of etch kinetics and mechanisms in low-pressure halogen-containing plasmas.

Kwang-Ho Kwon received his BS, MS, and PhD degrees in electrical engineering from Korea University, Seoul, Korea, in 1985, 1987, and 1993, respectively. From 1987 to 1995, he was with ETRI, where he was involved in the research and development of silicon semiconductor processing and plasma etching. From 1995 to 2005, he was an associate professor with the Department of Electronic Engineering of Hanseo University, Seosan, Korea. In 2005, he joined Korea University, where he is currently a professor of the Department of Control and Instrumentation Engineering. He is a member of the Electrochemical Society and IEEE. His research interests include plasma etching processes, silicon semiconductor processing, and sensor devices.